

Bipolar electron waveguides in graphene

R. R. Hartmann*

*Physics Department, De La Salle University,
2401 Taft Avenue, 0922 Manila, Philippines*

M. E. Portnoi†

*Physics and Astronomy, University of Exeter,
Stocker Road, Exeter EX4 4QL, United Kingdom and
ITMO University, St. Petersburg 197101, Russia*

Abstract

We show analytically that the ability of Dirac materials to localize an electron in both a barrier and a well can be utilized to open a pseudo-gap in graphene's spectrum. By using narrow top-gates as guiding potentials, we demonstrate that graphene bipolar waveguides can create a non-monotonous one-dimensional dispersion along the electron waveguide, whose electrostatically controllable pseudo-band-gap is associated with strong terahertz transitions in a narrow frequency range.

Graphene's gapless, relativistic spectrum leads to many unusual transport properties [1], such as Klein tunneling [2] and the suppression of back scattering [3]. Graphene also exhibits strong optical transitions, with a universal absorption of $\pi e^2/\hbar c \approx 2.3\%$ over a broad range of frequencies [4]. These defining features of graphene make electronic and optical control difficult to achieve. Indeed, for the realisation of optoelectronic devices which capitalize on the relative nature of graphene's dispersion, one must overcome certain undesirable relativistic features, without destroying all the attractive effects.

For optoelectronic devices applications, it would be highly desirable to modify graphene's spectrum such that it possesses valence-like and conduction-like bands, separated by an externally tunable pseudo-bandgap (a true gap would require a drastic modification of the material by either functionalization, cutting or rolling), as well as reduce the freedom of quasiparticle motion from two-dimensions down to one. In essence, we wish to form an analog of a narrow-gap carbon nanotube spectrum, without physically deforming the sheet by cutting it to make a ribbon, or rolling it to form a nanotube. Such a pseudo-gap would result in the giant enhancement of the probability of optical transitions across the gap [5]. However, unlike a nanotube or ribbon, whose bandgap is predefined by geometry, we seek to create a pseudo-gap which is fully tunable, without the need for huge magnetic fields [6, 7]. Rather than achieving the quantization of momentum through geometry like a nanoribbon, or nanotube does, one may instead quantize momentum via the application a quasi-one-dimensional (1D) electrostatically defined potential, i.e., by using electron waveguides [8–20]. Unlike a physical tube whose radius cannot be changed, externally applied potentials can be easily varied. There has been significant experimental progress since the pioneering work in the field of graphene electron waveguides [21–26] and the recent breakthrough of utilizing a nanotube as a top gates [27] enabled the detection of individual guided modes within a single waveguide. However, apart from graphene waveguides possessing a threshold in the characteristic potential strength required to observe a fully bound mode [14, 28], one could argue that a single graphene electron waveguides provides similar physics to that studied in quasi-1D channels within conventional semiconductor systems. Indeed, the absolute value of electron momentum along the direction of a waveguide formed by an attractive potential (quantum well) defines the electron's effective mass. Confined states of a deep well start with negative energy and for large values of momentum have a positive dispersion along the waveguide. Similarly, a potential barrier can also form a waveguide, where the confined

electron states have negative dispersion, i.e., are hole-like. This raises the question what happens when branches of negative and positive dispersion meet? Answering this question is the focus of this Letter. In what follows we show that a bipolar electronic waveguide is a fully tunable quasi-1D system with a non-monotonous dispersion accompanied by pseudo-gaps, characterized by a giant enhancement of density of states and interband dipole transition probabilities in the energy range where graphene's own density of states is rather small. In addition we present a general analytic formalism allowing us to find with a spectacular degree of accuracy the main features of a bipolar waveguide from the properties of a single quantum well.

Transmission through single and multiple barriers in graphene has been a subject of extensive research [2, 9, 21–23, 29–36] including periodic potentials [37] and sinusoidal multiple-quantum-well systems [38, 39]. Despite this significant body of research, the phenomenon of pseudo-gap formation in bipolar waveguides has been hitherto overlooked. It should be emphasized that the idea of using bipolar waveguides stems directly from the essential feature of graphene, as a gapless material, that a potential barrier can contain guided electron modes, effectively acting as a potential well. For non-relativistic particles, the probability of tunneling between two wells results in the splitting of energy levels, to form a doublet state. In contrast, the probability of tunneling between a well and a barrier in graphene results in the bands forming an avoided crossing at finite k_y , where $\hbar k_y$ is the momentum along the waveguide. As we demonstrate below, by modulating the applied voltage, bipolar waveguides have fully controllable pseudo-gaps, which exhibit extremely strong optical transitions. Not only this, but these transitions occur in the highly elusive and desirable THz frequency range. This part of the electromagnetic spectrum is notoriously difficult to generate and manipulate [40]. Therefore, by using a suitably chosen combination of guiding potentials, one can transform a graphene sheet into a narrow-gap nanotube without rolling, where the effective nanotube radius is controlled by the strength of the applied potential.

Inspired by the most advanced experimentally attainable waveguides [27], our proposed bipolar waveguide is defined by two nanotubes (top gates), of radius r_0 , separated by a distance d , as shown in Fig. 1 (a). Both nanotubes are placed at a height, h , above the metallic substrate. The potential profile in the graphene plane separated from the same

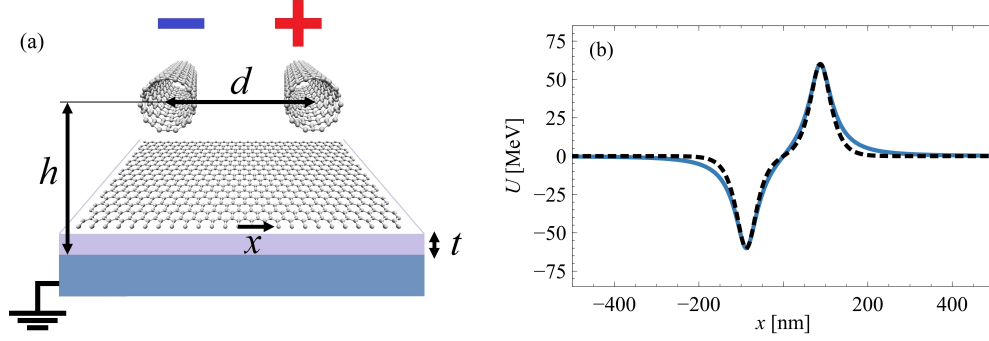


FIG. 1. (a) The schematic of the proposed experimental setup and (b) a comparison between the potential created by two nanotubes, separated a distance $d = 175$ nm, with $h = 40$ nm, and $t = 20$ nm (grey line) and the linear combination of a well and barrier defined by shifted $\pm u_0 / \cosh(x/L)$ functions (black dashed line) for the case of $\phi_1 = -\phi_2 = 0.25$ V, matching both their peak values and second-derivative at their maxima.

substrate by another distance t is given by the expression:

$$u(x) = \frac{e\tilde{\phi}_1}{2} \ln \left[\frac{(x + \frac{d}{2})^2 + (h - t)^2}{(x + \frac{d}{2})^2 + (h + t)^2} \right] + \frac{e\tilde{\phi}_2}{2} \ln \left[\frac{(x - \frac{d}{2})^2 + (h - t)^2}{(x - \frac{d}{2})^2 + (h + t)^2} \right], \quad (1)$$

where $\tilde{\phi}_{1,2} = \phi_{1,2} / \ln \left(\frac{2h - r_0}{r_0} \right)$, and ϕ_1 (ϕ_2) is the applied voltage between the left (right) nanotube and the back gate. The expression above can be easily modified when the top gates are fully embedded in a dielectric material. In the above-mentioned recent work [27], a smooth electron waveguide was fabricated using a carbon nanotube as a top gate and the graphene sheet was sandwiched in between two layers of hexagonal boron nitride (h-BN). The top h-BN layer had a thickness, h , of between 4 and 100 nm, and the bottom layer had a thickness, t of around 20 nm. It can be seen from Fig. 1 (b) that the potential in the plane of the graphene sheet, derived using image charges in the substrate, can be very well approximated by a linear combination of two shifted hyperbolic secant functions. It is convenient to use this particular approximation because for a single well, the hyperbolic secant potential possesses quasi-exact solutions to the Dirac equation [14, 16, 41]. This will enable us to treat both the size of the pseudo-gap and the optical transitions across it analytically.

The low-energy quasiparticle behaviour in graphene is known to be described with spectacular accuracy by the 2D Dirac equation for massless fermions [42]. In the presence of a confining electrostatic potential, $U(x)$, the effective 1D matrix Hamiltonian for confined

modes in a graphene waveguide can be written in the standard basis of graphene's two sub-lattices as

$$\hat{H} = \hbar v_F \left(\hat{k}_x \sigma_x + s_K k_y \sigma_y \right) + IU(x), \quad (2)$$

where $\hat{k}_x = -i \frac{\partial}{\partial x}$, k_y is a wavenumber corresponding to the motion along the waveguide, $\sigma_{x,y,z}$ are the Pauli spin matrices, I is the 2 by 2 unit matrix, v_F is the Fermi velocity, which is approximately $\approx 10^6$ m/s, and s_K is the valley quantum number, which has the value of +1 and -1 for the K and K' valley respectively.

We are interested in the situation when $U(x)$ is a combination of two fast decaying potentials separated by a distance d . For a better understanding of the underlying physics it is instructive to look both at the same and different sign constituent potentials. This allows a comparison with the familiar non-relativistic results for the double quantum well. The results are especially transparent for a quasi-one dimensional potential formed by a combination of either; a well and a barrier of the same strength, or, two equal wells:

$$U(x) = u\left(x + \frac{d}{2}\right) \pm u\left(x - \frac{d}{2}\right), \quad (3)$$

where, $u(x)$ is an individual symmetric potential well, for which the Hamiltonian, Eq. (2), admits exact zero-energy eigenfunctions, which we denote as $\Psi_0(x)$. The function $\Psi_0(x)$ is normalized and assumed to rapidly decay outside of the well. The tunneling between wells, or between a well and a barrier, results in the energy level, $E = 0$, splitting into two levels, E_1 and E_2 . At $E = 0$, the barrier wave function, denoted Ψ_- , is the complex conjugate of the well wave function, $\Psi_- = \Psi_0^*(x - \frac{d}{2})$, reflecting the fact that the barrier for electrons is a well for holes; whereas, for the two-well case $\Psi_+ = \Psi_0(x - \frac{d}{2})$. In the weak wavefunction overlap approximation, resembling the tight-binding (Hückel molecular orbital) methods widely used in solid-state and molecular physics, we may write the wave functions corresponding to eigenvalues E_1 and E_2 as:

$$\Psi_1 = \frac{1}{\sqrt{2}} \left[\Psi_{\pm} \left(x - \frac{d}{2} \right) + \Psi_0 \left(x + \frac{d}{2} \right) \right], \quad (4)$$

$$\Psi_2 = \frac{1}{\sqrt{2}} \left[\Psi_{\pm} \left(x - \frac{d}{2} \right) - \Psi_0 \left(x + \frac{d}{2} \right) \right]. \quad (5)$$

Following an approach similar to the non-relativistic case [43], but for a matrix Hamiltonian, the energy level splitting, $E_g = |E_2 - E_1|$, can be shown to be

$$E_g = 2\hbar v_F \left| \Psi_{\pm}^{\dagger} \left(-\frac{d}{2} \right) \sigma_x \Psi_0 \left(\frac{d}{2} \right) \right|. \quad (6)$$

It should be noted that there is a striking difference between the relativistic and non-relativistic case. For the non-relativistic case the splitting is proportional to the product of the single well function and its derivative [43]; whereas, in the relativistic case, it depends only on the individual well and barrier functions (or the two shifted well functions for the double well). For simplicity, we considered above two potentials of equal strengths, and estimated the splitting of the $E = 0$ state. These results can be easily generalized for non-equal potentials and non-zero values of energies as long as the energy levels in the individual potentials coincide (see supplementary information [44]). This theorem demonstrates the utility of quasi-exact solutions to the Dirac equation [14, 16, 28] for bipolar waveguides. Indeed, the exact solutions often correspond to the case where there is symmetry between the positive and negative energy solutions, allowing all pseudo-gaps to be treated within this formalism. Furthermore, knowledge of the exact wave-functions allows the matrix element of optical transitions across the pseudo-gaps to be calculated analytically.

In what follows we shall model a bipolar waveguide as

$$U(x) = -\frac{u_1}{\cosh \left[\left(x + \frac{d}{2} \right) / L \right]} + \frac{u_2}{\cosh \left[\left(x - \frac{d}{2} \right) / L \right]}. \quad (7)$$

For $u_1 = u_2 = u_0 > 0$, this smooth potential indeed provides an excellent fit to the realistic potential generated by two oppositely charged nanotubes above the surface of graphene, see Fig. 1 (b). Also each of the individual secant potentials supports exact analytic solutions at $E = 0$ [14], allowing the comparison of the numerical results with the approximate formula, Eq. (6). It is convenient to introduce similar dimensionless parameters as Ref. [14], namely $\omega = u_0/(\hbar v_F/L)$ and $\Delta = |k_y| L$. In the absence of inter-potential tunneling, the dispersion lines of the well and barrier (indicated in Fig. 2 by blue and red lines respectively) cross when $\Delta_n = \omega - n - 1/2$, where n is a positive integer [14]. The corresponding exact wavefunctions when substituted into Eq. (6) yield the following approximate expression for the $n = 0$ pseudo-gap (see supplementary information [44])

$$E_g/(\hbar v_F/L) \approx \frac{2 \exp(-\Delta_0 d/L)}{B(1 + \Delta_0, \Delta_0)}, \quad (8)$$

where $B(m, n)$ is the Beta function. This formula gives an extremely good approximation to the numerical solution in the limit when the ratio between the wire separation and the effective width of the potential is large, i.e., $d/L \gg 1$.

In Fig. 2 we plot the numerically obtained energy dependence on Δ , i.e. the momentum along the barrier in dimensionless units, for the cases of $\omega = 0.75$ (panel (a)) and $\omega = 1.75$

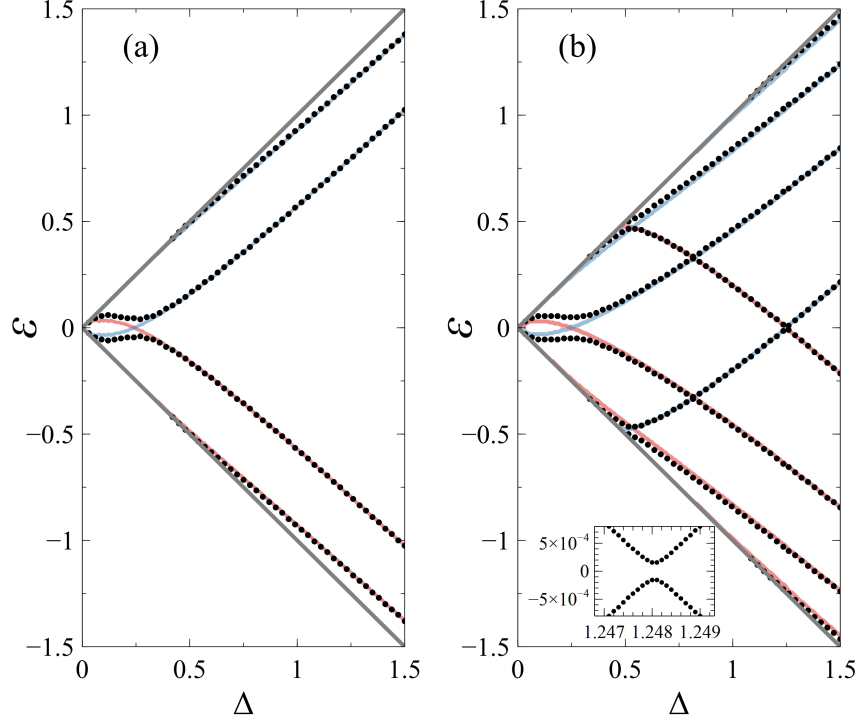


FIG. 2. The energy spectrum in dimensionless units, $\varepsilon = E/(\hbar v_F/L)$ vs $\Delta = |k_y|L$, of confined states in a bipolar waveguide (shown as black dotted lines), for a tube separation of $d/L = 8$ and a potential strength of (a) $\omega = u_0/(\hbar v_F/L) = 0.75$ and (b) $\omega = 1.75$. The blue and red lines show the dispersion lines for an isolated well and barrier respectively. The inset shows the detailed view of the second (for a larger value of Δ) zero-energy gap opening. The boundary at which the bound states merge with the continuum, $|E| = \hbar v_F |k_y|$, are denoted by the grey lines.

(panel (b)). In both cases the two oppositely charged nanotubes are separated by a distance $d/L = 8$, which corresponds to approximately 175 nm for the case of $h = 40$ nm and $t = 20$ nm. At this distance the energy-level splitting formula, Eq. (6), accurately predicts the value of the $n = 0$ pseudo-gap within a few per cent error. This error becomes one order of magnitude smaller when $d/L = 12$. It is instructive to compare these electrostatically induced pseudo-gaps with curvature-induced gaps in carbon nanotubes. For a narrow-gap carbon nanotube, it is well established that the larger is its radius, the smaller is the curvature-induced gap [45]. Therefore, the strength of the applied voltage, for a particular guided mode, can be mapped to the radius of the nanotube. Increasing the voltage results in more tightly confined guided modes, characterised by a higher value of Δ_0 entering Eq. (8), therefore we arrive to a smaller value of the pseudo-gap, which moves to the

right in Fig. 2. It can also be seen from the right panel of this figure that the deeper the well and higher the barrier, the more states are contained within each channel, increasing correspondingly the number of avoided crossings appearing in the dispersion. It should also be noted that although increasing the voltage leads to stronger confinement for lower order modes, it also results in the appearance of higher order modes which are more spread out, leading to additional wider pseudo-gaps. In Fig. 2 (b), which corresponds to the case of a deeper well and higher barrier, we can see two pseudo-gaps at $E = 0$ as well as additional pseudo-gaps at non-zero energy since there are more guided modes in the low-energy part of the spectrum.

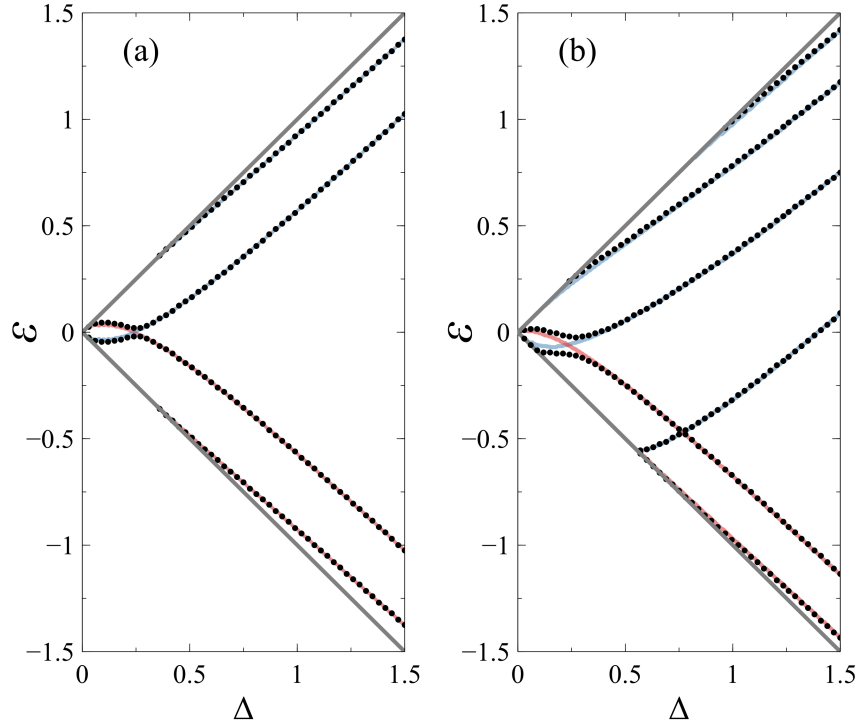


FIG. 3. The energy spectrum in dimensionless units, $\varepsilon = E/(\hbar v_F/L)$ vs $\Delta = |k_y|L$, of confined states in a bipolar waveguide (shown as black dotted lines), defined by the potential $-u_1/\cosh[(x + \frac{d}{2})/L] + u_2/\cosh[(x - \frac{d}{2})/L]$, for the case of (a) $u_1 = u_2 = 0.75 \hbar v_F/L$, $d/L = 12$ and (b) $u_1 = 1.9 \hbar v_F/L$, $u_2 = 0.6 \hbar v_F/L$, $d/L = 8$. The blue and red lines show the dispersion lines for an isolated well and barrier respectively, while the grey lines show the boundary at which the bound states merge with the continuum at $|E| = \hbar v_F |k_y|$.

It can be seen by comparing Fig. 3 (a) to Fig. 2 (a) that increasing the distance between the nanotubes, decreases the size of the gap. This is a result of the decrease in the overlap

between the well and barrier functions. Technologically it is quite difficult to have exact control over the precise tube separation. However, this is not so important since it is possible to control the value of the pseudo-gap by the applied voltage. Furthermore, it can be seen from Fig. 3 (b) that the effect of pseudo-gap opening is robust against asymmetry in the system. In Fig. 3 (b), the dispersion is recalculated for two tubes separated at the same distance as in Fig. 2 (a), but with the depth of the well increased to $\omega = 1.9$, while the size of the barrier decreased to $\omega = 0.6$. This demonstrates that top gates of mismatched radius, or dissimilar magnitudes of applied voltage will just shift the value in energy in which the avoided crossing occurs. Although Eqs. (6,8) give for the double well and bipolar waveguide the same value of energy-level splitting at the value of k_y corresponding to $E = 0$ in a single well, for the double well there is no pseudo-gap and the dispersion remains monotonous, this case is considered in depth elsewhere [46].

In what follows we shall demonstrate that much like in narrow-gap nanotubes [5], the wavefunction intermixing leads to strongly allowed optical transitions across the pseudo-gaps. The probability of optical transitions is proportional to the squared modulus of the matrix element of velocity operator between the relevant states. The velocity operator written in the same basis as the Hamiltonian given in Eq. (2) is [5, 47]

$$\langle \Psi_f | \hat{\mathbf{v}} | \Psi_i \rangle / v_F = \sigma_x e_x + s_K \sigma_y e_y, \quad (9)$$

where Ψ_i and Ψ_f are the initial and final states, respectively, and $\mathbf{e} = (e_x, e_y)$ is the light polarization vector. For linearly polarized light, $\mathbf{e} = (\cos(\varphi_0), \sin(\varphi_0))$, while for right- and left-handed polarized light $\mathbf{e} = (1, -i)/\sqrt{2}$ and $\mathbf{e} = (1, i)/\sqrt{2}$. Within the small wavefunction overlap approximation, for a bipolar waveguide defined by the potential given by Eq. (7) with $u_1 = u_2 = u_0 > 0$, the matrix element of velocity of the $n = 0$ mode at $\Delta = \Delta_0$ is [44]

$$|\langle \Psi_2 | \hat{\mathbf{v}} | \Psi_1 \rangle| / v_F \approx \left| \frac{e_x B\left(1 - e^{-d/L}; \frac{1}{2} + \Delta_0, 0\right) e^{-\Delta_0 d/L}}{B(1 + \Delta_0, \Delta_0)} - i \frac{k_y}{|k_y|} \frac{e_y B\left(\frac{1}{2} + \Delta_0, \frac{1}{2} + \Delta_0\right)}{B(1 + \Delta_0, \Delta_0)} \right|, \quad (10)$$

where $B(x; m, n)$ is the incomplete Beta function. For the case of the double well, at the same value of momentum, the matrix element of velocity of the $n = 0$ mode is the first term of Eq. (10), whereas $v_y = 0$. It reflects the fact that transitions in a double well are only caused by light polarized along the x -direction (normal to the waveguide), similar to the non-relativistic case.

In stark contrast, the transition across the pseudo-gap of a bipolar waveguide is strongly polarized along the y -axis (waveguide direction). The situation changes away from the pseudo-gap. For small values of $|k_y|$, the transitions are polarized normally to the y -direction, as expected from the momentum alignment phenomenon in graphene [47]. For large values of $|k_y|$, the overlap between the well and barrier wavefunctions becomes very small leading to vanishing transition probabilities for both polarizations. This effect very much resembles the situation in a narrow-gap carbon nanotube, where optical transitions polarized along the nanotube axis are allowed in the narrow energy interval around the curvature-induced gap [5]. The main difference from a nanotube can be clearly seen from Fig. 4, namely both transitions polarizations along and normal to the waveguide are allowed across the pseudo-gap. The contribution of the x -component exponentially decreases with an increase in top gate potential or the separation between the gates, as can be seen from Fig. 4.

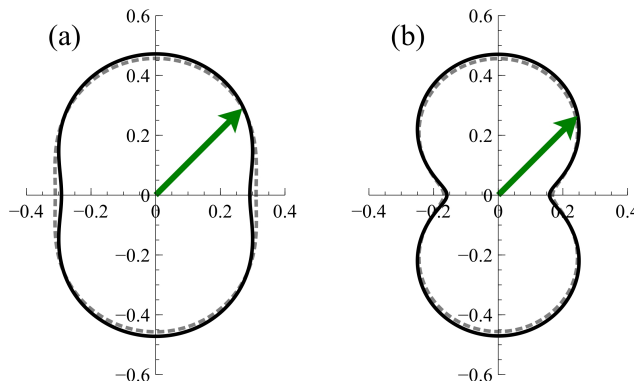


FIG. 4. Polar plots, showing the dependence of the absolute value (the length of the green arrow) of the velocity matrix element (in units of v_F) across the $n = 0$ pseudo-gaps for dipole transitions caused by normally-incident linearly polarized light on the angle between the polarization vector and the x -axis normal to the bipolar waveguide, defined by $\omega = 0.75$, for two different top gate separations: (a) $d/L = 8$ and (b) $d/L = 12$. The analytic approximation is depicted by the dashed grey line and the numerically obtained values are shown by the black solid line.

The presence of both polarizations for pseudo-gap transitions leads to an effect absent in both graphene and non-chiral nanotubes. Namely, right- and left-handed polarized light produces different populations of pseudo-valleys with opposite signs of k_y . This can be clearly seen from Eq. (10). This feature does not depend on the model describing the potential [44].

The discussed transitions across the pseudo-gap, fully controlled by the top gate voltages, can be easily brought into the highly desirable THz frequency range, which is usually extremely difficult to control. The presence of the van Hove singularity at the pseudo-gap edge enhances the strength of these transitions. These effects opens the avenue for novel gate-controlled polarized sensitive THz detectors based on bipolar waveguides in graphene.

To conclude, we have shown that bipolar waveguides allows for the creation of a non-monotonous 1D dispersion along the electron waveguide. The repulsion of well and barrier states results in the appearance of pseudo-gaps in the spectrum, whose size and symmetry can be fully controlled by the top gate voltages. These gaps can be estimated analytically for exactly-solvable potentials. The opening of these pseudo-gaps results in strongly allowed THz transitions with non-trivial optical selection rules. The predicted negative dispersion of the guided modes may lead to various other physical effects ranging from solitary waves [48] to Gunn-diode type current oscillations [49].

We thank C.A. Downing for his critical reading of the manuscript. This work was supported by the EU H2020 RISE project TERASSE (H2020-823878). RRH acknowledges financial support from URCO (71 F U 3TAY18-3TAY19). The work of MEP was supported by the Ministry of Science and Higher Education of Russian Federation, Goszadanie no. 2019-1246.

* richard.hartmann@dlsu.edu.ph

† M.E.Portnoi@exeter.ac.uk

- [1] A. H. Castro Neto, F. Guinea, N. M. R. Peres, K. S. Novoselov, and A. K. Geim, *Rev. Mod. Phys* **81**, 109 (2009).
- [2] M. I. Katsnelson, K. S. Novoselov, and A. K. Geim, *Nat. Phys* **2**, 620 (2006).
- [3] T. Ando, T. Nakanishi, and R. Saito, *J. Phys. Soc. Jpn* **67**, 2857 (1998).
- [4] R. R. Nair, P. Blake, A. N. Grigorenko, K. S. Novoselov, T. J. Booth, T. Stauber, N. M. R. Peres, and A. K. Geim, *Science* **320**, 1308 (2008).
- [5] R. R. Hartmann, V. A. Saroka, and M. E. Portnoi, *J. Appl. Phys* **125**, 151607 (2019).
- [6] M. E. Portnoi, O. V. Kibis, and M. R. Da Costa, *Superlattices Microstr.* **43**, 399 (2008).
- [7] R. R. Hartmann and M. E. Portnoi, in *IOP Conf. Ser.: Mater. Sci. Eng*, Vol. 79 (2015) pp.

12014–12018.

- [8] J. M. Pereira Jr, V. Mlinar, F. M. Peeters, and P. Vasilopoulos, Phys. Rev. B **74**, 045424 (2006).
- [9] V. V. Cheianov, V. Fal’ko, and B. L. Altshuler, Science **315**, 1252 (2007).
- [10] T. Y. Tudorovskiy and A. V. Chaplik, JETP Lett. **84**, 619 (2007).
- [11] A. V. Shytov, M. S. Rudner, and L. S. Levitov, Phys. Rev. Lett. **101**, 156804 (2008).
- [12] C. W. J. Beenakker, R. A. Sepkhanov, A. R. Akhmerov, and J. Tworzydło, Phys. Rev. Lett. **102**, 146804 (2009).
- [13] F.-M. Zhang, Y. He, and X. Chen, Appl. Phys. Lett **94**, 212105 (2009).
- [14] R. R. Hartmann, N. J. Robinson, and M. E. Portnoi, Phys. Rev. B **81**, 245431 (2010).
- [15] L. Zhao and S. F. Yelin, Phys. Rev. B **81**, 115441 (2010).
- [16] R. R. Hartmann and M. E. Portnoi, Phys. Rev. A **89**, 012101 (2014).
- [17] Y. He, Y. Xu, Y. Yang, and W. Huang, Appl. Phys. A **115**, 895 (2014).
- [18] H. Hasegawa, Physica E Low Dimens. Syst. Nanostruct. **59**, 192 (2014).
- [19] Y. Xu and L. K. Ang, J. Opt **17**, 035005 (2015).
- [20] Y. Xu and L. K. Ang, Electronics **5**, 87 (2016).
- [21] B. Huard, J. A. Sulpizio, N. Stander, K. Todd, B. Yang, and D. Goldhaber-Gordon, Phys. Rev. Lett. **98**, 236803 (2007).
- [22] B. Özyilmaz, P. Jarillo-Herrero, D. Efetov, D. A. Abanin, L. S. Levitov, and P. Kim, Phys. Rev. Lett. **99**, 166804 (2007).
- [23] R. V. Gorbachev, A. S. Mayorov, A. K. Savchenko, D. W. Horsell, and F. Guinea, Nano Lett. **8**, 1995 (2008).
- [24] G. Liu, J. Velasco Jr, W. Bao, and C. N. Lau, Appl. Phys. Lett **92**, 203103 (2008).
- [25] J. R. Williams, T. Low, M. S. Lundstrom, and C. M. Marcus, Nat. Nanotechnol **6**, 222 (2011).
- [26] P. Rickhaus, M.-H. Liu, P. Makk, R. Maurand, S. Hess, S. Zihlmann, M. Weiss, K. Richter, and C. Schönenberger, Nano Lett. **15**, 5819 (2015).
- [27] A. Cheng, T. Taniguchi, K. Watanabe, P. Kim, and J.-D. Pillet, Phys. Rev. Lett. **123**, 216804 (2019).
- [28] R. R. Hartmann and M. E. Portnoi, Sci. Rep **7**, 1 (2017).
- [29] V. V. Cheianov and V. I. Falko, Phys. Rev. B **74**, 041403 (2006).
- [30] J. R. Williams, L. DiCarlo, and C. M. Marcus, Science **317**, 638 (2007).

- [31] J. M. Pereira Jr, P. Vasilopoulos, and F. M. Peeters, Appl. Phys. Lett **90**, 132122 (2007).
- [32] J. M. Pereira Jr, P. Vasilopoulos, and F. M. Peeters, Microelectronics J **39**, 534 (2008).
- [33] J. M. Pereira Jr, F. M. Peeters, A. Chaves, and G. A. Farias, Semicond. Sci. Technol **25**, 033002 (2010).
- [34] H. Bahlouli, E. B. Choubabi, A. Jellal, and M. Mekkaoui, J. Low Temp. Phys **169**, 51 (2012).
- [35] A. D. Alhaidari, H. Bahlouli, and A. Jellal, Adv. Theor. Math. Phys. **2012** (2012).
- [36] D. Wei-Yin, Z. Rui, X. Yun-Chang, and D. Wen-Ji, Chin. Phys. B **23**, 017202 (2013).
- [37] L. Brey and H. A. Fertig, Phys. Rev. Lett. **103**, 046809 (2009).
- [38] G. J. Xu, X. G. Xu, B. H. Wu, J. C. Cao, and C. Zhang, J. Appl. Phys **107**, 123718 (2010).
- [39] C. H. Pham and V. L. Nguyen, J. Phys. Condens. Matter **27**, 095302 (2015).
- [40] M. Lee and M. C. Wanke, Science **316**, 64 (2007).
- [41] R. R. Hartmann, I. A. Shelykh, and M. E. Portnoi, Phys. Rev. B **84**, 035437 (2011).
- [42] P. R. Wallace, Phys. Rev. **71**, 622 (1947).
- [43] L. D. Landau and E. M. Lifshitz, *Quantum mechanics: non-relativistic theory*, Vol. 3 (Elsevier, 2013).
- [44] See Supplementary Information.
- [45] C. L. Kane and E. J. Mele, Phys. Rev. Lett. **78**, 1932 (1997).
- [46] R. R. Hartmann and M. E. Portnoi, arXiv preprint arXiv:2008.10798 (2020).
- [47] V. A. Saroka, R. R. Hartmann, and M. E. Portnoi, arXiv preprint arXiv:1811.00987 (2018).
- [48] D. R. Gulevich, D. Yudin, D. V. Skryabin, I. V. Iorsh, and I. A. Shelykh, Sci. Rep **7**, 1 (2017).
- [49] J. B. Gunn, Solid State Commun. **1**, 88 (1963).